Infectious Disease Modelling 7 (2022) 742–760

Contents lists available at ScienceDirect

Infectious Disease Modelling

journal homepage: www.keaipublishing.com/idm

Host movement, transmission hot spots, and vector-borne disease dynamics on spatial networks

Omar Saucedo [a, *], Joseph H. Tien [b]

[a] Department of Mathematics, Virginia Tech, Blacksburg, VA, USA
[b] Department of Mathematics, The Ohio State University, Columbus, OH, USA

ARTICLE INFO

Article history:
Received 12 April 2022
Received in revised form 4 September 2022
Accepted 26 October 2022
Available online 4 November 2022

Keywords:
Human movement
Vector-borne disease
Spatial networks
Reproduction number
Laurent series

ABSTRACT

We examine how spatial heterogeneity combines with mobility network structure to influence vector-borne disease dynamics. Specifically, we consider a Ross-Macdonald-type disease model on n spatial locations that are coupled by host movement on a strongly connected, weighted, directed graph. We derive a closed form approximation to the domain reproduction number using a Laurent series expansion, and use this approximation to compute sensitivities of the basic reproduction number to model parameters. To illustrate how these results can be used to help inform mitigation strategies, as a case study we apply these results to malaria dynamics in Namibia, using published cell phone data and estimates for local disease transmission. Our analytical results are particularly useful for understanding drivers of transmission when mobility sinks and transmission hot spots do not coincide.

1. Introduction

Vector-borne diseases affect approximately one billion people and account for 17% of all infectious diseases (Tibayrenc, 2017). Understanding the spatial dynamics of vector-borne diseases is crucial, particularly in the context of increased mobility linking disparate geographic locations (Qiu, Kong, Li, & Martcheva, 2013), changes in mobility patterns due to urbanization, economic development, and globalization, and ecological and environmental changes affecting vector abundance (Chen, 2017; Sutherst, 2004). The interaction between mobility networks and local transmission characteristics is complex. Many factors influence local transmission characteristics, including host demography, host density, ecological conditions for the vector (e.g. vegetation, rainfall and temperature, breeding sites), vector abundance, economic resources (e.g. window screens, bed nets), and much more (Bousema et al., 2010; Mbogo et al., 2003). Spatial locales additionally differ in terms of their connectivity. Host movement patterns can include the presence of central 'hubs' serving to link distinct locales, 'source' locales with migration patterns reflecting urbanization, new connections with previously remote locales due to development and changes in land usage, and more (Hay, Guerra, Tatem, Atkinson, & Snow, 2005; Matthys et al., 2006). Understanding how these myriad factors combine to influence disease dynamics is challenging, particularly given widespread heterogeneity in habitat suitability and connectivity between locales. For example, it is possible for movement patterns to allow disease to

* Corresponding author.
E-mail address: osaucedo@vt.edu (O. Saucedo).
Peer review under responsibility of KeAi Communications Co., Ltd.

https://doi.org/10.1016/j.idm.2022.10.006

persist in areas where vector abundance is low (Cosner, 2015). Other work has shown that host movement can lead to disease extinction even in the presence of disease hot spots (Smith, Dushoff, & McKenzie, 2004). Thus it is a delicate question how network structure and local disease characteristics combine to affect vector-borne disease dynamics.

There is an extensive literature on using metapopulation models for studying infectious disease dynamics (Arino & van den Driessche, 2006; Ball et al., 2015; Citron et al., 2007; Hanski, 1999; Pei, Kandula, & Shaman, 2020; Rohani, Earn, & Grenfell, 1999; Xia, Bjørnstad, & Grenfell, 2004), including for vector-borne diseases (Adams & Kapan, 2009; Barrios, Lee, & Vasilieva, 2018; Cosner, 2015; Cosner et al., 2009; Gaff & Gross, 2007; Gao et al., 2014; Mpolya, Yashima, Ohtsuki, & Sasaki, 2014; Mukhtar, Munyakazi, & Ouifki, 2020; Ruktanonchai et al., 2016a; Smith et al., 2014; Torres-Sorando & Rodriguez, 1997). We do not attempt to give a comprehensive review here, but instead simply mention some of the key concepts in the context of the present work. A fundamental issue is how heterogeneity and connectivity between spatial locations combine to affect disease dynamics, including disease invasion (Bichara, Iggidr, & Yacheur, 2021; Cosner, 2015; Gao, 2019; Gao & Ruan, 2012; Wang, 2007; Zhang, 2020) and persistence (Acevedo et al., 2015; Adams & Kapan, 2009; Hasibeder & Dye, 1988), outbreak size and duration (Citron et al., 2007; Manore et al., 2015), and timing and synchrony between locations (Althouse et al., 2012; Churakov, Villabona-Arenas, Kraemer, Salje, & Cauchemez, 2019). Particular considerations for vector-borne diseases include potentially different movement scales between host and vector (Auger, Kouokam, Sallet, Tchuente, & Tsanou, 2008; Smith et al., 2014), vector population dynamics including seasonality (Aron et al., 1982; Chitnis, Hardy, & Smith, 2012; Hoshen & Morse, 2004) and multi-species interactions (Gao & Ruan, 2012; Reiner et al., 2013), interventions targeting vector and host (Agusto et al., 2013; Demers et al., 2020; Hughes & Britton, 2013; Paton et al., 2019), and challenges for model parameterization (Guerra et al., 2014; Ruktanonchai et al., 2016b; Tatem et al., 2014). Many different modeling approaches have been taken for examining these questions, including compartmental models (Acevedo et al., 2015; Bichara & Castillo-Chavez, 2016), agent-based models (Bomblies, 2014; Jindal & Rao, 2017; Mniszewski, Manore, Bryan, Del Valle, & Roberts, 2014), network models (Kirkland, Shuai, van den Driessche, & Wang, 2021; Lippi et al., 2020; Zhao, Liu, & Zhang, 2021), stochastic models (Le, Kumar, & Ruiz, 2018; Maliyoni, Chirove, Gaff, & Govinder, 2017; Son & Denu, 2021), and more. For a review of approaches for modeling spatial connectivity and mosquito-borne disease dynamics, see (Lee, Jarvis, Edmunds, Economou, & Lowe, 2021).

The primary objective of this manuscript is to present analytical tools for understanding how network structure and local characteristics combine to influence vector-borne disease dynamics. The impact of heterogeneity and connectivity on the domain reproduction number and control efforts has been studied for specific network types, such as two patch networks (Acevedo et al., 2015; Auger et al., 2008), lattices (Caraco, Duryea, Glavanakov, Maniatty, & Szymanski, 2001; Demers et al., 2020; Schwab, Stone, Fonseca, & Fefferman, 2018), star graphs (Mpolya et al., 2014), and bipartite graphs (Bisanzio et al., 2010; Iggidr, Sallet, & Souza, 2016; Zhang, 2020). One of the contributions of our work is that we derive analytical results for an arbitrary strongly connected graph with arbitrary patch-specific parameters. Specifically, Tien et al. (Tien, Shuai, Eisenberg, & van den Driessche, 2015) give techniques for computing the domain reproduction number for a network SIR-type model with environmental pathogen movement. Their methods involve a Laurent series expansion in the next generation matrix approach to computing $\mathcal{R}_0$. Here we adapt this approach to the vector-borne disease setting. We consider a network Ross-Macdonald (Smith et al., 2012) type model, and derive an approximation for the domain $\mathcal{R}_0$ in terms of an average of the patch $\mathcal{R}_0$ values in isolation, where the average is taken with respect to a probability measure that combines network structure and local pathogen removal rates. We then use this average to compute sensitivities of the domain $\mathcal{R}_0$ to parameters such as the local transmission and recovery rates. As an illustration of how these results can be used in practice, we consider malaria in Namibia as a case study. We use cell phone data from (Ruktanonchai et al., 2016b) to estimate host movement between health districts, and use published estimates based upon the Malaria Atlas Project for parameterizing local disease characteristics (Gething et al., 2011). We then compute sensitivities of the domain $\mathcal{R}_0$ for malaria in Namibia based upon these data and our analytical results. These sensitivities can be useful for guiding intervention strategies. In particular, our methods give a way to combine information on movement sources and sinks with disease hot spots to assess disease dynamics on the domain. The Namibia malaria case study also highlights the increasingly available data on mobility patterns and local disease transmission that can be used to apply analytical and computational methods to help understand vector-borne disease dynamics and inform intervention efforts.

We use an Eulerian framework for modeling host movement, and assume that vectors do not move between spatial locations. This situation may be reasonable on large spatial scales, where connectivity for hosts occurs through automobile and air traffic, but vector dispersal on this spatial scale is rare (Adams & Kapan, 2009; Stoddard et al., 2009; Sumner, Orton, Green, Kao, & Gubbins, 2017). The Eulerian framework corresponds to migration between nodes. This is in contrast with Lagrangian frameworks for movement, corresponding to commuting between nodes from a distinguished home location. Both approaches are widely used. For discussion and comparison of these frameworks, see (Cosner et al., 2009; Hasibeder & Dye, 1988; Gueron, Levin, & Rubenstein, 1996; Rodriguez & Torres-Sorando, 2001; Vargas Bernal, Saucedo, & Tien, 2022). An advantage of the Eulerian approach is tractability for mathematical analysis, such as approximation to the domain reproduction number using the techniques of (Tien et al., 2015). The cell phone data from (Ruktanonchai et al., 2016b) that we use for our Namibia case study are in the form of a mixing matrix for a Lagrangian framework. Vargas Bernal et al. (Vargas Bernal, Saucedo, & Tien, 2022) present an approach for relating the Eulerian and Lagrangian modeling frameworks for vector-borne disease models through a fundamental matrix. We use this approach here to estimate a mobility matrix from the Namibia cell phone data, and then analyze the resulting Eulerian model to compute sensitivities of the domain reproduction number to

local transmission and recovery parameters. Our work thus illustrates how the techniques of (Tien et al., 2015) and (Vargas Bernal, Saucedo, & Tien, 2022) can be used together in practice.

The remainder of this article is structured as follows. In Section 2 we present the modeling framework that will be used throughout. Section 3 gives our analytical results. Background material on graph theory, random walks on graphs, and key results from (Tien et al., 2015) that serve as foundation for our analysis are given in Section 6.1. After establishing some preliminary results in Section 3.1, we derive an approximation for the domain $\mathcal{R}_0$ using a Laurent series expansion in Section 3.2. We calculate the sensitivities of this approximation of the domain $\mathcal{R}_0$ to the model parameters in Section 3.3, and apply these results to malaria in Namibia in Section 4. We conclude with a discussion in Section 5.

2. Model description

We consider vector-host disease dynamics on n discrete spatial locations. Disease dynamics within each location follows a Ross-Macdonald-type model (Reiner et al., 2013; Ross, 1916), with coupling through host movement. Host movement follows an Eulerian (Cosner, 2015; Cosner et al., 2009; Gueron et al., 1996) framework. The resulting system of equations is similar to the Eulerian model considered in (Cosner, 2015; Cosner et al., 2009), but with the inclusion of host vital dynamics, allowing for different host mobility networks depending upon immunological status, and assuming that vectors do not move. Results by (Cosner et al., 2009) include establishing global stability of the disease free equilibrium for $\mathcal{R}_0 < 1$ and for the endemic equilibrium when $\mathcal{R}_0 > 1$.

Disease dynamics within a single location follows the flow diagram in Fig. 1. Let S_i^h and I_i^h denote the number of susceptible and infectious hosts in location i, respectively, and let S_i^v and I_i^v denote the number of susceptible and infectious vectors. Let N_i^h and N_i^v denote the total host and vector populations in location i, respectively. For simplicity, we do not explicitly consider a latent stage for either host or vector. We also assume there is no infection-derived immunity for hosts. This is consistent with diseases such as malaria (Doolan, Dobaño, & Baird, 2009), and the SIS-SI system that we use as a building block here has been used previously in malaria modeling studies (Smith et al., 2004).

Let a_i denote the per capita biting rate of vectors on hosts in location i, let b correspond to the probability that a bite by an infected vector on a susceptible host results in infection of the host, and let c denote the probability that a bite by a susceptible vector on an infected host results in infection of the vector. We assume an incubation period for vectors of length τ. Per capita mortality rates for host and vector in location i are denoted by μ_i^h and μ_i^v, respectively. As in the Ross-Macdonald framework, we assume frequency-dependent transmission with transmission parameter from vector to host in location i as $\beta_i^h = a_i b e^{-\mu_i^v \tau}$, and transmission parameter from host to vector in location i as $\beta_i^v = a_i c$. Infected hosts recover at rate γ_i^h.

Let m_{ij}^x denote the per capita movement rate of individuals of type x from location j to location i, where $x \in \{S, I\}$. $M^x = [m_{ij}^x]$ is thus the weighted adjacency matrix for the mobility network for individuals of type x. Our subsequent analysis will focus on M^I, the mobility network for infectious hosts. We will assume throughout that M^I is irreducible (Assumption (A3) below). This corresponds to a strongly connected mobility network for infectious hosts: for any ordered pair (j, i), there is a path starting from j and terminating at i.

We thus have a network of nodes, each with SIS-SI vector-host dynamics and linked to one another through host movement. Fig. 1 shows a schematic. Note that we are placing minimal constraints on the host mobility network, with the only constraint that the mobility network for I be strongly connected. Note also that the parameters are allowed to vary between nodes, allowing for heterogeneity in local disease transmission, vector abundance, demography, health care access, and environmental conditions. Thus the framework we consider is flexible, allowing examination of how network structure and local transmission dynamics interact to affect vector-host disease dynamics on the network.

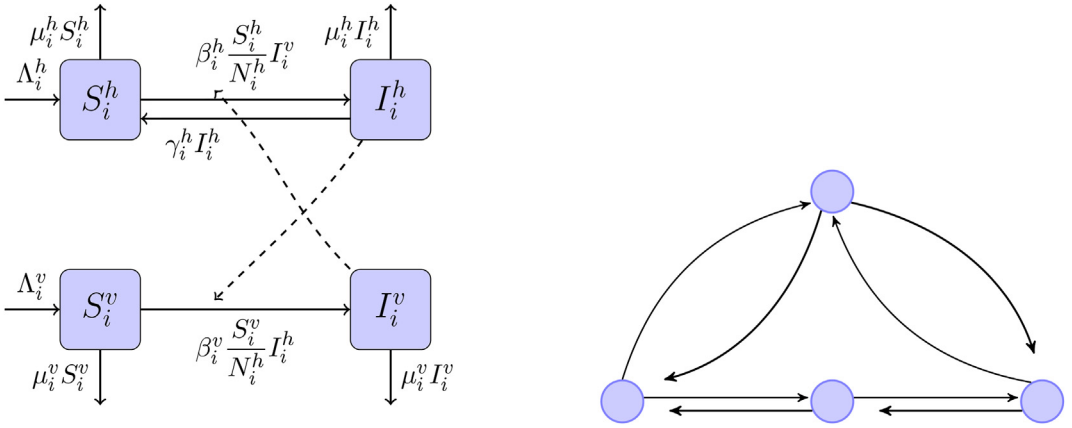

Fig. 1. *Left:* Model dynamics within each spatial location. *Right:* Schematic of network dynamics for system (2.1). Each node corresponds to a spatial location with SIS-SI dynamics within location. Nodes are connected by host movement. Vectors are assumed not to move.

The resulting system of ordinary differential equations is given in (2.1):

$$\begin{aligned}
\frac{dS_i^h}{dt} &= \Lambda_i^h - \beta_i^h \frac{S_i^h}{N_i^h} I_i^v - \mu_i^h S_i^h + \sum_{j=1}^{n} m_{ij}^S S_j^h - \sum_{j=1}^{n} m_{ji}^S S_i^h + \gamma_i^h I_i^h, \\
\frac{dI_i^h}{dt} &= \beta_i^h \frac{S_i^h}{N_i^h} I_i^v - \left(\mu_i^h + \gamma_i^h\right) I_i^h + \sum_{j=1}^{n} m_{ij}^I I_j^h - \sum_{j=1}^{n} m_{ji}^I I_i^h, \\
\frac{dS_i^v}{dt} &= \Lambda_i^v - \beta_i^v \frac{S_i^v}{N_i^h} I_i^h - \mu_i^v S_i^v, \\
\frac{dI_i^v}{dt} &= \beta_i^v \frac{S_i^v}{N_i^h} I_i^h - \mu_i^v I_i^v,
\end{aligned} \tag{2.1}$$

for $i = 1, \ldots, n$.

Model parameters and variables are summarized in Table 1. We make the following assumptions throughout the manuscript:

A1: The parameters Λ_i^h, Λ_i^v, μ_i^h, and μ_i^v are positive.
A2: The parameters β_i^h, β_i^v, and γ_i^h are non-negative.
A3: M^I is irreducible.

3. Analysis

This section focuses on deriving expressions for $\mathcal{R}_0$ and looking at the sensitivity of $\mathcal{R}_0$ to different parameters. The technical approach is that introduced in Tien et al. (2015), where a Laurent series expansion is given for the fundamental matrix V^{-1} in the next generation matrix. Central to this is the interplay between movement and removal ("absoption") on the network. A generalized inverse of the graph Laplacian called the *absorption inverse* plays a key role in this analysis (Jacobsen &

Table 1
Model parameters for system (2.1). The subscript i denotes the ith patch.

Parameter	Description
S_i^h	Number of susceptible host in patch i.
I_i^h	Number of infected host in patch i.
R_i^h	Number of recovered host in patch i.
S_i^v	Number of susceptible vector in patch i.
I_i^v	Number of infected vector in patch i.
Λ_i^h	Host recruitment rate in patch i.
β_i^h	Transmission rate from vector to host in patch i
μ_i^h	Host death rate in patch i.
γ_i^h	Host per capita recovery rate in patch i.
d_i	Host removal rate $\mu_i^h + \gamma_i^h$ from patch i.
Λ_i^v	Vector recruitment rate in patch i.
β_i^v	Transmission rate from host to vector in patch i.
μ_i^v	Vector per capita death rate in patch i.
m_{ij}^k	The per capita movement rate of the host moving from patch j to patch i from compartment $k = S, I$, or R.
a	The number of bites on humans, per mosquito, per day.
b	The transmission efficiency from mosquitoes to humans. (i.e. probability of infection from mosquitoes to humans).
c	The transmission efficiency from humans to mosquitoes. (i.e. probability of infection from humans to mosquitoes).
τ	Vector incubation period.
G_i	Transfer matrix with respect to the compartments $i = S, I$, or R.
A	Adjacency matrix.
W	Diagonal out-degree matrix of A.
L	Unnormalized graph Laplacian.
u	Strictly positive basis vector of ker L with $\sum_{i=1}^{n} u_i = 1$.
$\bar{d}$	Average host removal rate $\sum_{i=1}^{n} d_i u_i$.
D	Diagonal absorption matrix with entries d_i.

Tien, 2018). After some preliminaries (Section 3.1), we use Laurent series expansion in Section 3.2 to derive a closed form expression that approximates the domain $\mathcal{R}_0$. This $\mathcal{R}_0$ expression involves averaging according to a probability measure that combines network structure and pathogen removal rates at the different spatial locations, and can be used to compute approximate sensitivities of $\mathcal{R}_0$ to model parameters. These sensitivities are given in Section 3.3.

3.1. Preliminaries

Our analysis makes extensive use of the graph Laplacian for host movement. We recall the definition of the (unnormalized) graph Laplacian here for the convenience of the reader. Let $A \in \mathbb{R}^{n\times n}$ be the adjacency matrix for a weighted, directed graph G and let A_{ij} define the weight of the arc from j to i. The (unnormalized) graph Laplacian of G is

$$L = W - A, \tag{3.1}$$

where W is diagonal with $W_{ii} = \sum_{k=1}^{n} A_{ki}$.

As a preliminary to computing $\mathcal{R}_0$ for system (2.1), let us first consider the reproduction number for a single node in isolation. We have the standard result from applying the next generation matrix:

$$\mathcal{R}_{0,i} = \sqrt{\frac{\beta_i^v \beta_i^h}{(\mu_i^h + \gamma_i^h)\mu_i^v}}. \tag{3.2}$$

Let L_x be the graph Laplacian of the mobility network for individuals of type $x \in \{S, I\}$. Define

$$\begin{aligned} G_S &= L_S + D_\mu, \\ G_I &= L_I + D_{\mu+\gamma}, \end{aligned} \tag{3.3}$$

where $D_\mu = \text{diag}\{\mu_i^h\}$ and $D_{\mu+\gamma} = \text{diag}\{\mu_i^h + \gamma_i^h\}$.

Solving for the disease-free equilibrium (DFE) of the system (2.1), we have:

$$\Lambda_i^h - \mu_i^h S_i^h + \sum_{j=1}^{n} m_{ij}^S S_j^h - \sum_{j=1}^{n} m_{ji}^S S_i^h = 0, \tag{3.4}$$

$$\Lambda_i^v - \mu_i^v S_i^v = 0. \tag{3.5}$$

Equation (3.4) yields $G_S S = \Lambda$, where $S = (S_1^h, \ldots, S_n^h)^T$ and $\Lambda = (\Lambda_1^h, \ldots, \Lambda_n^h)^T$. Notice that (A1) implies that G_S has the Z-sign pattern (i.e. all off-diagonal entries are less than or equal to zero (Horn & Johnson, 1986)) with positive diagonal entries, and thus G_S is a nonsingular M-matrix (e.g. properties D_{16} and I_{29} in (Berman & Plemmons, 1994)). Thus,

$$S^* = G_S^{-1}\Lambda, \tag{3.6}$$

where $S^* = (S_1^{h^*}, \ldots, S_n^{h^*})^T$ and $G_S^{-1} \geq 0$ by (Berman & Plemmons, 1994).

From (3.5) and (A1), we have $S_i^{v^*} = \Lambda_i^v/\mu_i^v$. Therefore, the DFE for system (2.1) is

$$(S_1^{h^*}, 0, S_1^{v^*}, 0, S_2^{h^*}, 0, S_2^{v^*}, \ldots, S_n^{h^*}, 0, S_n^{v^*}, 0)^T.$$

3.2. Approximating the domain $\mathcal{R}_0$ via laurent series expansion

We now consider the domain $\mathcal{R}_0$ for system (2.1) using the next generation matrix (van den Driessche & Watmough, 2002). Using the Laurent series approach of (Tien et al., 2015), we show that to lowest order, the domain reproduction number can be approximated by a simple expression involving the expectation of the square of the reproduction numbers for each patch in isolation, where the expectation is taken with respect to a probability measure that involves both network structure and the local pathogen removal rates.

Ordering the variables in system (2.1) as $(I_1^h, \ldots, I_n^h, I_1^v, \ldots, I_n^v)$, we have

$$\mathcal{F} = \begin{pmatrix} \frac{\beta_1^h S_1^h I_1^v}{N_1^h} \\ \vdots \\ \frac{\beta_n^h S_n^h I_n^v}{N_n^h} \\ \frac{\beta_1^v S_1^v I_1^h}{N_1^h} \\ \vdots \\ \frac{\beta_n^v S_n^v I_n^h}{N_n^h} \end{pmatrix}, \quad \mathcal{V} = \begin{pmatrix} (\mu_1^h + \gamma_1^h) I_1^h - \sum_{j=1}^n m_{1j} I_j^h + \sum_{j=1}^n m_{j1} I_1^h \\ \vdots \\ (\mu_n^h + \gamma_n^h) I_n^h - \sum_{j=1}^n m_{nj} I_j^h + \sum_{j=1}^n m_{jn} I_n^h \\ \mu_1^v I_1^v \\ \vdots \\ \mu_n^v I_n^v \end{pmatrix}. \tag{3.7}$$

Linearizing $\mathcal{F}$ and $\mathcal{V}$ at the DFE gives:

$$F = \begin{pmatrix} 0 & D_\beta \\ D_{\beta_v} & 0 \end{pmatrix}, \text{ and } V = \begin{pmatrix} G_I & 0 \\ 0 & D_{\mu_v} \end{pmatrix},$$

where

$$D_\beta = \operatorname{diag}\left\{\beta_1^h, \ldots, \beta_n^h\right\}, \tag{3.8}$$

$$D_{\beta_v} = \operatorname{diag}\{\beta_1^v, \ldots, \beta_n^v\}, \tag{3.9}$$

$$D_{\mu+\gamma} = \operatorname{diag}\left\{\mu_1^h + \gamma_1^h, \ldots, \mu_n^h + \gamma_n^h\right\}, \tag{3.10}$$

$$D_{\mu_v} = \operatorname{diag}\{\mu_1^v, \ldots, \mu_n^v\}. \tag{3.11}$$

Note that G_I is a nonsingular M-matrix with $G_I^{-1} > 0$. The next generation matrix is thus

$$FV^{-1} = \begin{pmatrix} 0 & D_\beta (D_{\mu_v})^{-1} \\ D_{\beta_v} G_I^{-1} & 0 \end{pmatrix}. \tag{3.12}$$

We now study the spectral radius of (3.12) using a Laurent series expansion for G_I^{-1}. It will be useful to write G_I in terms of $z = \max\{\mu_i^h + \gamma_i^h\}$, where z is a measure of how quickly pathogen is removed from the nodes of the network. Then we can write G_I as

$$G_I = L_I + z\overline{D}_{\mu+\gamma}, \tag{3.13}$$

where $\overline{D}_{\mu+\gamma} = D_{\mu+\gamma}/\max\{\mu_i^h + \gamma_i^h\}$. Thus $z > 0$ is a parameter describing the scale of infected host removal, and the entries of $\overline{D}_{\mu+\gamma}$ describe the relative removal rates of infected hosts between the nodes. We can consider the effect of varying z while the relative removal rates of infected hosts between nodes is fixed.

It is useful to interpret the transfer matrix V in terms of an absorbing random walk, where absorption corresponds to permanent pathogen removal (for example, through infected host recovery or death). Let L_I^d denote the absorption inverse of L_I with respect to the absorption rates

$$d_i = \mu_i^h + \gamma_i^h. \tag{3.14}$$

Properties of the absorption inverse are given in (Jacobsen & Tien, 2018). From (Jacobsen & Tien, 2018), for $|z| < 1/\rho(L_I^d \overline{D}_{\mu+\gamma})$ we can express the matrix G_I^{-1} as a Laurent series:

$$G_I^{-1} = \frac{1}{z} U + L_I^d + \sum_{k=1}^{\infty} \left(-z L_I^d \overline{D}_{\mu+\gamma}\right)^k L_I^d, \tag{3.15}$$

where $U = \frac{u\mathbf{1}^T}{\overline{d}}$, $u = (u_1, \ldots, u_n)^T$ is a basis for the nullspace of L_I with $u > 0$ and $\sum_{i=1}^n u_i = 1$, and $\overline{d}$ given by

$$\overline{d} = \sum_{i=1}^{n} u_i d_i. \tag{3.16}$$

Note that u corresponds to the stationary distribution of the random walk on the host mobility network generated by L_l, and thus reflects the structure of the host mobility network. We define G_I^{-1} as the fundamental matrix of the absorbing random walk generated by G_I (Dobrow, 2016).

Now consider the eigenvalues of FV^{-1}. We use the following lemma to exploit the block structure of (3.12).

Lemma 3.2.1. *Let $A, B, C, D \in M_{n\times n}(\mathbb{R})$. Suppose A is invertible and $AC = CA$. Then*

$$\det\begin{pmatrix} A & B \\ C & D \end{pmatrix} = \det(AD - CB).$$

Proof. Under the assumption that A invertible, we have

$$\begin{pmatrix} A^{-1} & 0 \\ -C & A \end{pmatrix}\begin{pmatrix} A & B \\ C & D \end{pmatrix} = \begin{pmatrix} I & A^{-1}B \\ -CA + AC & AD - CB \end{pmatrix}. \tag{3.17}$$

Taking the determinant of both sides and using that $AC = CA$ gives

$$\begin{aligned} &\det\begin{pmatrix} A^{-1} & 0 \\ -C & A \end{pmatrix}\det\begin{pmatrix} A & B \\ C & D \end{pmatrix} \\ &\quad = \det\begin{pmatrix} I & A^{-1}B \\ 0 & AD - CB \end{pmatrix} \\ &\quad = \det(AD - CB). \end{aligned} \tag{3.18}$$

Next, as the determinant is transpose invariant, we have

$$\det\begin{pmatrix} A^{-1} & 0 \\ -C & A \end{pmatrix} = \det\begin{pmatrix} A^{-t} & -C^t \\ 0 & A^t \end{pmatrix} = \det(A^{-1}A) = 1, \tag{3.19}$$

so

$$\det\begin{pmatrix} A & B \\ C & D \end{pmatrix} = \det(AD - CB). \blacksquare$$

Using Lemma 3.2.1, we have that

$$\det\left(FV^{-1} - \lambda I\right) = \det\begin{pmatrix} -D_\lambda & D_\beta D_{\mu_v}^{-1} \\ D_{\beta_v} G_I^{-1} & -D_\lambda \end{pmatrix} \tag{3.20}$$

$$= \det\left(D_\lambda^2 - D_{\beta_v} G_I^{-1} D_\beta D_{\mu_v}^{-1}\right), \tag{3.21}$$

so the eigenvalues of the matrix $D_{\beta_v} G_I^{-1} D_\beta D_{\mu_v}^{-1}$ are the square of the eigenvalues of FV^{-1}. As the matrix $D_{\beta_v} G_I^{-1} D_\beta D_{\mu_v}^{-1}$ is similar to the matrix $G_I^{-1} D_\beta D_{\mu_v}^{-1} D_{\beta_v}$, it suffices to find the eigenvalues of the matrix $G_I^{-1} D_\beta D_{\mu_v}^{-1} D_{\beta_v}$.

We now use the Laurent series (6.4) for G_I^{-1} for finding approximate eigenvalues for $G_I^{-1} D_\beta D_{\mu_v}^{-1} D_{\beta_v}$. Let

$$\hat{D} = D_\beta D_{\mu_v}^{-1} D_{\beta_v} = \operatorname{diag}\frac{\beta_1^h \beta_1^v}{\mu_1^v}, \ldots, \frac{\beta_n^h \beta_n^v}{\mu_n^v}, \tag{3.22}$$

and consider the approximation for G_I^{-1} using only the lowest order term in (6.4). Then we have

$$G_I^{-1}\hat{D} \approx \frac{1}{z} U\hat{D}. \tag{3.23}$$

Note that U is rank 1 and $\hat{D}$ has full rank, implying that $\frac{1}{z}U\hat{D}$ has only one nonzero eigenvalue, which we can directly compute:

$$\begin{aligned}\frac{1}{z}U\hat{D}u &= \frac{1}{z}\frac{u\mathbf{1}^T}{\overline{d}}\hat{D}u \\ &= \frac{1}{z}\frac{1}{\overline{d}}u\mathbf{1}^T(\hat{D}_{11}u_1,\ldots,\hat{D}_{nn}u_n)^T \\ &= \frac{1}{z}\left(\frac{\sum_{i=1}^n \hat{D}_{ii}u_i}{\overline{d}}\right)u. \end{aligned} \tag{3.24}$$

Thus, the spectral radius of $D_{\beta_v}G_I^{-1}D_{\beta}D_{\mu_v}^{-1}$ is approximately $\frac{1}{z}(\sum_{i=1}^n \hat{D}_{ii}u_i)/\overline{d}$.

Substituting (3.22) and (6.6) for $\hat{D}$ and $\overline{d}$, respectively, and using (3.2), we have the following lowest order approximation to the domain reproduction number:

$$\begin{aligned}\mathcal{R}_0 &\approx \frac{1}{\sqrt{z}}\sqrt{\sum_{i=1}^n \hat{D}_{ii}u_i\frac{1}{\overline{d}}} \\ &= \frac{1}{\sqrt{z}}\sqrt{\sum_{i=1}^n \frac{\beta_i^h\beta_i^v u_i}{\mu_i^v}\frac{1}{\overline{d}}} \\ &= \frac{1}{\sqrt{z}}\sqrt{\sum_{i=1}^n \frac{\beta_i^h\beta_i^v}{\mu_i^v(\mu_i^h+\gamma_i^h)}d_iu_i\frac{1}{\overline{d}}} \\ &= \frac{1}{\sqrt{z}}\sqrt{\sum_{i=1}^n \left[\mathcal{R}_{0,i}\right]^2 d_iu_i\frac{1}{\overline{d}}} \\ &= \frac{1}{\sqrt{z}}\sqrt{\mathrm{E}\left[\mathcal{R}_{0,i}^2\right]} \\ &:= \hat{\mathcal{R}}_0, \end{aligned} \tag{3.25}$$

where $d_i = \mu_i^h + \gamma_i^h$ and the expectation of $\mathcal{R}_{0,i}^2$ is with respect to the probability measure $d_iu_i/\overline{d}$. As pointed out in (Jacobsen & Tien, 2018), this probability measure corresponds to the stationary distribution of the random walk generated by the Laplacian for the 'absorption-scaled graph'. Expression (3.25) is the analogue to the approximation obtained in (Tien et al., 2015) for 'SIWR' systems (Tien & Earn, 2010) coupled by environmental pathogen movement, and shows how network structure (through the u_i in the probability measure) and local node characteristics (the node-specific removal rates d_i, and the node-specific reproduction numbers) combine to shape the domain $\mathcal{R}_0$. Note that in the vector-borne disease setting (2.1), $\hat{\mathcal{R}}_0$ involves the square root of the expectation of the square of the reproduction numbers for each patch in isolation.

3.3. Sensitivity analysis

The closed form approximation for the domain $\mathcal{R}_0$ in (3.25) allows us to probe how network structure and local disease characteristics combine to affect disease dynamics. In this section we use (3.25) to examine the sensitivity of the domain $\mathcal{R}_0$ to model parameters. This can help in evaluating the potential impact of intervention strategies.

For sufficiently small z, we can approximate the sensitivity of $\mathcal{R}_0$ to parameter p by differentiating the expression in (3.25) with respect to p and multiplying by the normalizing term $\frac{p}{\mathcal{R}_0}$ as in (Chitnis, Hyman, & Cushing, 2008). This yields the following scaled sensitivities:

$$\frac{\partial\mathcal{R}_0}{\partial\beta_i^h}\frac{\beta_i^h}{\mathcal{R}_0} \approx \frac{\partial\hat{\mathcal{R}}_0}{\partial\beta_i^h}\frac{\beta_i^h}{\hat{\mathcal{R}}_0} = \frac{1}{2z}\frac{1}{\sqrt[3]{\hat{\mathcal{R}}_0}}\left[\mathcal{R}_{0,i}\right]^2\frac{d_iu_i}{\overline{d}}, \tag{3.26}$$

$$\frac{\partial\mathcal{R}_0}{\partial\beta_i^v}\frac{\beta_i^v}{\mathcal{R}_0} \approx \frac{\partial\hat{\mathcal{R}}_0}{\partial\beta_i^v}\frac{\beta_i^v}{\hat{\mathcal{R}}_0} = \frac{1}{2z}\frac{1}{\sqrt[3]{\hat{\mathcal{R}}_0}}\left[\mathcal{R}_{0,i}\right]^2\frac{d_iu_i}{\overline{d}}, \tag{3.27}$$

$$\frac{\partial \mathcal{R}_0}{\partial \gamma_i^h}\frac{\gamma_i^h}{\mathcal{R}_0} \approx \frac{\partial \hat{\mathcal{R}}_0}{\partial \gamma_i^h}\frac{\gamma_i^h}{\hat{\mathcal{R}}_0} = -\frac{1}{2}\sqrt{\hat{\mathcal{R}}_0}\left(\frac{\gamma_i^h u_i}{\bar{d}}\right), \tag{3.28}$$

$$\frac{\partial \mathcal{R}_0}{\partial \mu_i^v}\frac{\mu_i^v}{\mathcal{R}_0} \approx \frac{\partial \hat{\mathcal{R}}_0}{\partial \mu_i^v}\frac{\mu_i^v}{\hat{\mathcal{R}}_0} = -\frac{1}{2z}\frac{1}{\sqrt[3]{\hat{\mathcal{R}}_0}}[\mathcal{R}_{0,i}]^2\frac{d_i u_i}{\bar{d}}. \tag{3.29}$$

Each of the expressions in (3.26) - (3.29) shows how network structure and local dynamics combine to shape the $\mathcal{R}_0$ sensitivities. In particular, we see that the relative sensitivities between nodes of $\mathcal{R}_0$ to a given parameter are determined either by $\mathcal{R}_{0,i}^2 d_i u_i$ (for the sensitivities to the transmission parameters β_i^h, β_i^v, and to the vector mortality rates μ_i^v) or $\gamma_i^h u_i$ (for the sensitivity to the host recovery rates γ_i^h).

Determining effective intervention strategies in the context of heterogeneous local transmission and complex mobility networks is challenging. The sensitivities (3.26)–(3.29) can be useful for evaluating intervention efforts such as vector elimination (e.g. increasing μ_i^v in targeted locations), bed net distribution (e.g. decreasing β_i^h and β_i^v), or chemotherapy following infection (e.g. increasing γ_i^h) (Sutherst, 2004). We illustrate this first in Section 3.3.1 for a toy example, to show the interaction between transmission hot spots and mobility sources and sinks. We then turn to an empirical case study of malaria dynamics in Namibia in Section 4.

3.3.1. Toy example

A practical consideration regarding vector-borne disease dynamics is the role that mobility sources, mobility sinks, and transmission hot spots play in driving transmission. In the 'strongly coupled' regime where the Laurent series is well-approximated by the first term, the sensitivities (3.26)–(3.29) can be used to disentangle this, as the sensitivity expressions include terms reflecting network structure (u_i), local transmission dynamics ($\mathcal{R}_{0,i}$), and host removal ("absorption rates", d_i). The d_i appear in the sensitivities (3.26), (3.27), and (3.29) as the product $d_i u_i$, which can be viewed as an *effective network structure* term taking absorption rates into account. Indeed, the $d_i u_i$ correspond to the stationary distribution of a random walk on the *absorption-scaled graph* introduced in (Tien et al., 2015). We illustrate how all these characteristics influence $\hat{\mathcal{R}}_0$ (and thus, for sufficiently small z, $\mathcal{R}_0$) with a set of toy examples.

Consider a two-node network, letting the local $\mathcal{R}_{0,i}$ values be fixed and taking node two as a transmission hot spot ($\mathcal{R}_{0,2} > 1$). A schematic is shown in Fig. 2, with red denoting the transmission hot spot (node 2), horizontal arrows

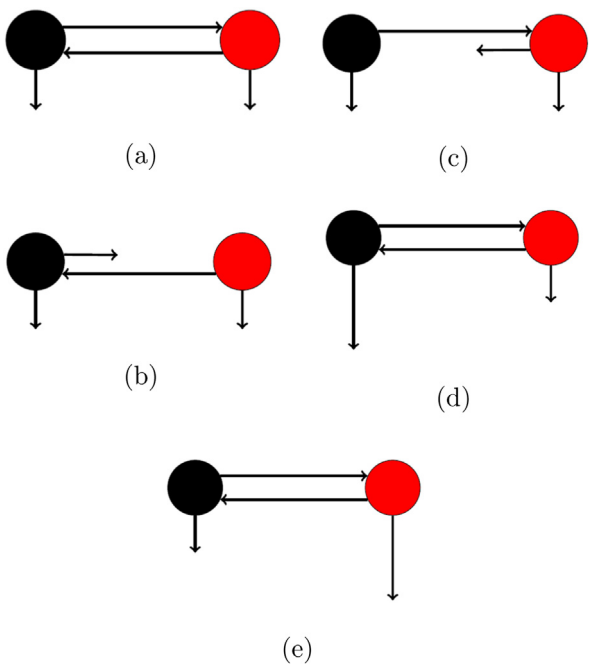

Fig. 2. Toy example illustrating the relationship between the patch specific reproduction numbers, network structure through u_i, and host absorption rates. Node 1 = black, node 2 = red. Red signifies a transmission hot spot. For all cases, $\mathcal{R}_{0,1} < 1 < \mathcal{R}_{0,2}$. We set up five scenarios in which we change the movement rates m_{ij} and the effective network structure $d_i u_i$. In the cases where the effective network structure terms are not equal, we assume the transmission rates are higher in node 2 in order to preserve the assumption of node 2 being a transmission hot spot. (a) movement rates are equal ($m_{12} = m_{21}$) and the effective network structure terms are equal ($d_1 u_1 = d_2 u_2$), (b) movement rates between the nodes are different ($m_{12} > m_{21}$) and the effective network structure terms are distinct ($d_1 u_1 > d_2 u_2$, $d_1 = d_2$), (c) movement rates between the nodes are different ($m_{12} < m_{21}$) and the effective network structure terms are distinct ($d_1 u_1 < d_2 u_2$, $d_1 = d_2$) (d) movement rates are equal ($m_{12} = m_{21}$) and the effect network structure terms are distinct ($d_1 u_1 > d_2 u_2$, $u_1 = u_2$) (e) movement rates are equal ($m_{12} = m_{21}$) and the effect network structure terms are distinct ($d_1 u_1 < d_2 u_2$, $u_1 = u_2$).

corresponding to movement between nodes, and vertical arrows corresponding to absorption. We assume that as the absorption rates vary (for example, between (a) and (d)), the transmission rates compensate in order to keep $\mathcal{R}_{0,i}$ fixed. We now consider several scenarios. In the first three cases, we vary the movement rates and the effective network structure terms by changing u_i. In (a), we have a network with equal movement rates $m_{12} = m_{21}$ and equal absorption rates between the nodes. Thus the effective network structure terms $d_i u_i$ are equal, and according to (3.26), (3.27), and (3.29), $\hat{\mathcal{R}}_0$ is more sensitive to the transmission parameters β_i^h, β_i^v and vector mortality rate (μ_i^v) in the transmission hot spot (node two). However (3.28) indicates that the sensitivity of $\hat{\mathcal{R}}_0$ to the host recovery rates γ_i^h are approximately equal between nodes. These results suggest that for balanced networks (i.e. networks where all the patches have equal net inflow and net outflow), with equal absorption rates, targeting transmission hot spots for interventions affecting transmission rates and vector mortality will lead to the largest reductions in $\hat{\mathcal{R}}_0$. In contrast, interventions that increase host recovery rates (for example, through increased treatment rates) will lead to comparable reductions in $\hat{\mathcal{R}}_0$ regardless of where the intervention is applied.

In (b), we consider an unbalanced network with $m_{12} > m_{21}$ and $d_1 = d_2$. In the language of (Tatem et al., 2014), node one is a mobility *sink*, and node two is a mobility *source*. This situation corresponds to $u_1 > u_2$, and the transmission hot spot corresponds to a mobility source on the absorption-scaled graph. Whether $\hat{\mathcal{R}}_0$ is more sensitive to the transmission $\left(\beta_i^h, \beta_i^v\right)$ and vector mortality (μ_i^v) parameters for node one versus node two depends upon the specific numerical values of u_i and $\mathcal{R}_{0,i}$. Thus further details are necessary for determining where to target interventions affecting β_i^h, β_i^v, and μ_i^v.

In (c), we switch the mobility rates so that node one is the mobility source, and node two the mobility sink (i.e. $m_{12} < m_{21}$) and again let $d_1 = d_2$. Here the transmission hot spot corresponds to a mobility sink on the absorption-scaled graph. $\hat{\mathcal{R}}_0$ is more sensitive to the parameters in node two compared to node one since we have that $\mathcal{R}_{0,1} u_1 < \mathcal{R}_{0,2} u_2$ for the transmission and removal parameters. Thus interventions at nodes that are simultaneously mobility sinks and transmission hot spots are likely to lead to relatively large reductions in domain $\hat{\mathcal{R}}_0$ when targeting transmission and removal terms.

In (d) and (e) we set $m_{12} = m_{21}$, but let $d_1 \neq d_2$. It is possible for the transmission hot spot to correspond to a mobility sink on the absorption-scaled graph, in which case $\hat{\mathcal{R}}_0$ is more sensitive to all the parameters in a transmission hot spot. This case is shown in (d). It is also possible for the transmission hot spot to correspond to a mobility source on the absorption-scaled graph. In this case the relative sensitivities of $\hat{\mathcal{R}}_0$ to β_i^h, β_i^v, and μ_i^v in node one versus two depend upon the specific numerical values for $\mathcal{R}_{0,i}$ and $d_i u_i$.

4. Case study: malaria in Namibia

We turn now to a case study of malaria in Namibia to illustrate how the techniques we have developed can be applied in practice. Data for this section are described in (Ruktanonchai et al., 2016b). Notably (Ruktanonchai et al., 2016b), provides both detailed empirical data on host mobility through cell phone records, as well as parameter estimates for local disease transmission characteristics through the Malaria Atlas Project. These are precisely the types of data required for applying our methods for approximating the domain $\mathcal{R}_0$ and examining its sensitivities to model parameters for evaluating intervention strategies. The mobility data from (Ruktanonchai et al., 2016b) are in the form of a mixing matrix directly suitable for a Lagrangian modeling framework. We will follow the approach established in (Vargas Bernal, Saucedo, & Tien, 2022) to associate the Eulerian and Lagrangian frameworks by relating the 'residence times' for the two models.

4.1. Mobility network

Ruktanonchai et al. (Ruktanonchai et al., 2016b) use anonymized cell phone records involving 9 billion communications sent by 1.19 million unique SIM cards in 2010 to estimate mobility patterns in Namibia. Locations were determined to the health district level (level 2 shapefile for Namibia given by Database of Global Administrative Areas) based upon cell tower corresponding to last communication for each day. Movement between health districts was estimated from changes in cell tower locations between communications, and resident health districts for each SIM card were estimated from most frequent location over a one year period. Communication records were then aggregated across SIM cards to estimate a mixing matrix $P = (p_{ij})_{n\times n}$ giving the proportion of time that a resident of j spent in i. The matrix P is a non-negative matrix with column sums equal to 1. For additional details, see (Ruktanonchai et al., 2016b).

We wish to use the mixing matrix P to estimate the adjacency matrix M^I in (2.1) for movement of infected hosts. While the majority of the data likely come from individuals whose movement is not affected by illness, we make the simple assumption here that the aggregate cell phone data from which P is computed are representative of movement for infected individuals. Illness has the potential to significantly impact movement patterns (Lin, Deger, & Tien, 2016). Further understanding of how illness affects movement and identifying data streams for estimating mobility patterns for infected individuals are important areas for future work.

The mixing matrix estimated by (Ruktanonchai et al., 2016b) is suitable for a Lagrangian modeling framework (Cosner et al., 2009). To adapt to the Eulerian framework used in (2.1), we use the idea of (Vargas Bernal, Saucedo, & Tien, 2022) to relate the two modeling frameworks through the expected 'residence times' of the two frameworks. We briefly describe our approach below; further details on this approach and comparison of the Lagrangian and Eulerian frameworks in the context of vector-borne disease is given in (Vargas Bernal, Saucedo, & Tien, 2022). Specifically, we do so by matching the expected times that individuals from j spend in i in both models. For system (2.1), the i, j entry of $(L + D_{\mu+\gamma})^{-1}$ corresponds to the expected time an (infectious) host in j spends in i, while the empirically estimated p_{ij} corresponds to the proportion of

time a resident of j spends in i. Multiplying this proportion by the infectious period $1/(\mu_j^h + \gamma_j^h)$ gives the expected time that an infectious resident of j spends in i. Equating these two expressions gives

$$(L + D_{\mu+\gamma})^{-1} = PD_{\mu+\gamma}^{-1}. \tag{4.1}$$

Given P and $D_{\mu+\gamma}$, it remains to estimate L. We do so by using the Frobenius norm to treat this as a constrained least squares problem, in the case where P is invertible (as is indeed the case for the Namibia cell phone data). Suppose that P invertible, and let $\hat{P}^{-1} = PD_{\mu+\gamma}^{-1}$. Let $\|\cdot\|_F$ denote the Frobenius norm. Then with (3.1) we have

$$\begin{aligned}
\min_{A\geq 0} \|(L + D_{\mu+\gamma})^{-1} - \hat{P} - 1\|_F &= \min_{A\geq 0} \|L + D_{\mu+\gamma} - \hat{P}\|_F \\
&= \min_{A\geq 0} \|W - A + D_{\mu+\gamma} - \hat{P}\|_F \\
&= \min_{A\geq 0} \|W - A - \left(D_{\mu+\gamma}P^{-1} - D_{\mu+\gamma}\right)\|_F \\
&= \min_{A\geq 0} \|W - A - D_{\mu+\gamma}\left(P^{-1} - I\right)\|_F.
\end{aligned} \tag{4.2}$$

In the case where all of the absorption rates are the same, $D_{\mu+\gamma}$ is equal to a scalar multiple of the identity and (4.2) can be written as

$$\min_{A\geq 0} \|\hat{W} - \hat{A} - (P^{-1} - I)\|_F, \tag{4.3}$$

where $W = \hat{W}D_{\mu+\gamma}$ and $A = \hat{A}D_{\mu+\gamma}$.

Numerical solutions to (4.3) were computed in MATLAB R2018A using the constrained linear least squares function lsqlin. The resulting estimated adjacency matrix for Namibia based upon the cell phone data is shown in Fig. 3.

As discussed in (Vargas Bernal, Saucedo, & Tien, 2022), (4.3) may not have a solution corresponding to zero. In the language of (Vargas Bernal, Saucedo, & Tien, 2022), such a situation is said to be *inconsistent*, and this is the case for the Namibia data. To examine how closely the estimated adjacency matrix M^I matches the original cell phone data, we consider the partial rank correlation coefficients between the entries of $(L + D_{\mu+\gamma})^{-1}$ and $\hat{P}^{-1}$ (Marino, Hogue, Ray, & Kirschner, 2008). The resulting partial rank correlation coefficients are shown in Fig. 4 (computations were done using the `partialcorr` function in MATLAB). From Fig. 4, we observed that over 90% of the PRCCs are above the value 0.90.

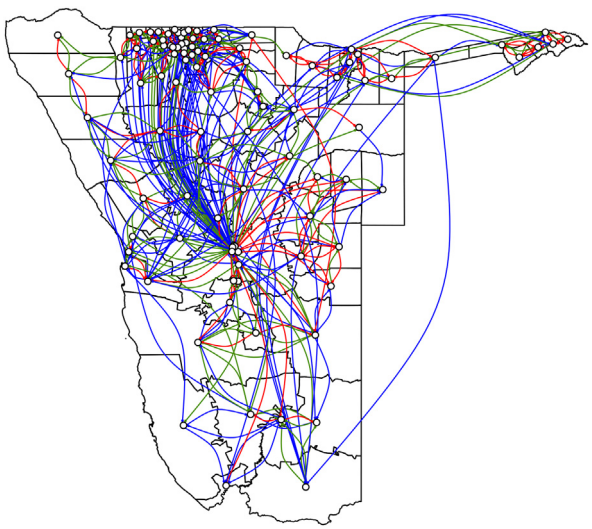

Fig. 3. The estimated connectivity network for Namibia. The distinct color lines on the map represent the level of connectivity between each region. The blue lines indicate a weak connectivity ($A_{ij} < 0.019$), the green lines represent an intermediate level of connectivity ($0.019 < A_{ij} < 0.039$), and the red lines denote strong connectivity ($A_{ij} > 0.039$). To avoid an overcrowded graph, we show values $A_{ij} > 0.01$.

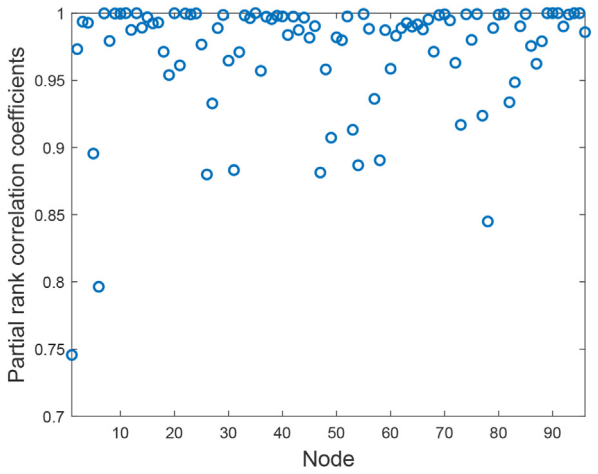

Fig. 4. Partial rank correlation coefficients (PRCC) between the empirically observed mixing matrix based upon cell phone data from (Ruktanonchai et al., 2016b), and residence times $(L+D)^{-1}$ for system (2.1). The majority of the PRCC values are above 0.90.

4.2. Local transmission parameters

Parameters for each health district were based upon estimates from (Ruktanonchai et al., 2016b), who used data from the Malaria Atlas Project to parameterize a Ross-Macdonald SIS model in a Lagrangian framework for host movement. Specifically, Ruktanonchai et al. give estimates of 0.3 for the human feeding rate of mosquitoes per day, 0.1 for the probability of transmitting from mosquito to human, 0.214 for the probability of transmitting from human to mosquito, 10 days for the incubation period, 0.1 per day for the death rate for mosquito, and 1/150 per day for the recovery rate of humans (Ruktanonchai et al., 2016b). We additionally estimate the host mortality rate to be 1/23002 per day from census data for Namibia (Plecher, 2018).

Ruktanonchai et al. (Ruktanonchai et al., 2016b) estimate the local reproduction numbers $\mathcal{R}_{0,i}$ based on malaria incidence data reported in the Malaria Atlas Project, assuming that disease is at steady state. We use their estimated local reproduction numbers for system (2.1) here. Values for the transmission parameters β_i, $\beta_{v,i}$ were then made assuming that these parameter values were equal within a given health district.

4.3. Sensitivity analysis

We now apply the sensitivity equations (3.26) - (3.29) to the Namibia data. Note that a necessary prerequisite for using the sensitivity equations is for the scale parameter z to be within the radius of convergence of the Laurent series (6.4), which is equivalent to $1 < \frac{1}{\rho(L^d D_{\mu+\gamma})}$. This is indeed the case here, with $\frac{1}{\rho(L^d D_{\mu+\gamma})} = 7.54$, well within the radius of convergence.

As noted in Section 3.3, the relative sensitivities between health districts depend upon $\mathcal{R}_{0,i} d_i u_i$ (for sensitivity to β_i^h, β_i^v, and μ_i^v) and $\gamma_i^h u_i$ (for sensitivity to γ_i). Here we use the same absorption rates d_i and recovery rates γ_i^h across health districts (Table 2), so the relative sensitivities are determined by the patch reproduction numbers $\mathcal{R}_{0,i}$ and the network structure through u_i. Fig. 5a and b shows $\mathcal{R}_{0,i}$ and u_i by health district, respectively. Note that the health districts with high within-patch transmissibility (dark blue, Fig. 5a) tend to be distinct from the health districts with high values of u_i (dark blue, Fig. 5b). This is consistent with the findings reported by (Ruktanonchai et al., 2016b) regarding transmission hot spots versus mobility sinks

Table 2
Parameters values for system (2.1) used for the malaria Namibia case study. Note that the transmission parameters for the host and vector range from 0 to 0.0279. Source: (Ruktanonchai et al., 2016b).

Parameter	Value	Units
β_i^h	$[0, 0.0279]$	days^{-1}
μ_i^h	$\frac{1}{23002}$	days^{-1}
γ_i^h	$\frac{1}{150}$	days^{-1}
β_i^v	$[0, 0.0279]$	days^{-1}
μ_i^v	$\frac{1}{10}$	days^{-1}

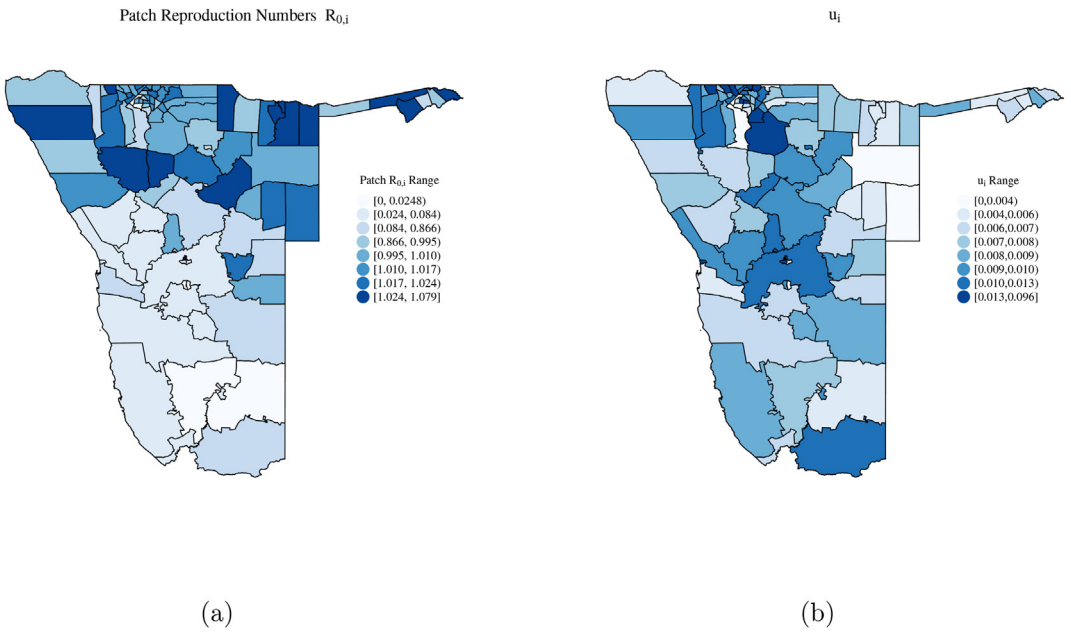

Fig. 5. (a) Reproduction numbers for each health district in isolation, as estimated by (Ruktanonchai et al., 2016b). (b) Values for the network structure through u_i by health district.

and sources. For example (Ruktanonchai et al., 2016b), report high patch reproduction numbers and disease prevalence in several rural northern health districts. By contrast, mobility sinks correspond to urban areas.

Comparison of patch reproduction numbers $\mathcal{R}_{0,i}$ and network structure through u_i in Fig. 5 shows differences in which health districts correspond to transmission hot spots (high $\mathcal{R}_{0,i}$; Fig. 5a) compared to health districts corresponding to mobility sinks (high u_i; Fig. 5b). Transmission hot spots are found in rural health districts in the northeastern part of the country. For example, the highest patch reproduction numbers are found in the Rundu Rural West, Rundu Rural East, Mashare, and Mpungu health districts. By contrast, mobility sinks are found in urban areas, with the highest values for u_i corresponding to Windhoek West, Oshakati East, Rundu Urban, and Katima Muliro Urban.

Fig. 6 shows the relative sensitivities of $\hat{\mathcal{R}}_0$ to β_i^h (Fig. 6a) and γ_i^h (Fig. 6b). From sensitivity equations (3.26), (3.29), and from our assumption that the host recovery rates γ_i^h and absorption rates d_i are equal through each health district, it is expected to observe similar maps in Fig. 6a and c. However as discussed in Section 3.3.1, the relative sensitivities of $\hat{\mathcal{R}}_0$ to β_i^h, β_i^v, and μ_i^v are determined by a combination of network structure and local transmission characteristics, via the $\mathcal{R}_{0,i}d_iu_i$ terms in (3.26) - (3.27) and (3.29). For the Namibia data, the four health districts where the domain $\hat{\mathcal{R}}_0$ is most sensitive to these parameters are Oshakati East, Katima Muliro Urban, Rundu Urban, and Ondangwa. Note that these health districts do not correspond to the four highest transmission hot spots, nor do they correspond to the ordering of the four highest mobility sinks (although Oshakati East, Katima Muliro Urban, and Rundu Urban are among the four health districts with highest u_i values). Thus intervention efficacy in terms of local transmission (β_i^h, β_i^v) and vector removal (μ_i^v) is not determined by mobility sinks and transmission hot spots independently of one another, but upon a combination of these factors. By contrast, the relative sensitivities to host recovery γ_i^h depends only upon the network structure through u_i in this case study (see equation (3.28)) as we assumed the host recovery rates to be equal. The consequence of having equal host recovery parameters can be seen in the similarities of Figs. 5b and 6b.

The sensitivities shown in Fig. 6 were computed from (3.26)-(3.29), which in turn are based upon the lowest term in the Laurent series expansion (6.4). The accuracy of these sensitivities thus depends upon the scale parameter z in (6.4). To examine the robustness of our conclusions from the sensitivities shown in Fig. 6, we examine how numerically computed sensitivities vary over a range of values for z. Fig. 7 shows how numerically computed sensitivity rankings for β_i^h, γ_i^h, and μ_i^v change over a range of z values. The rankings show very little change for $z < 0.01$, which includes the estimated z value of 0.0067 from the Namibia cell phone data (dashed line). These findings indicate that conclusions from the sensitivity equations (3.26)-(3.29) are informative for the parameter ranges considered.

5. Discussion

Disentangling the effects of network structure and transmission hot spots is a fundamental issue for understanding infectious disease dynamics. The analytical results presented in this paper can help elucidate how network structure and local

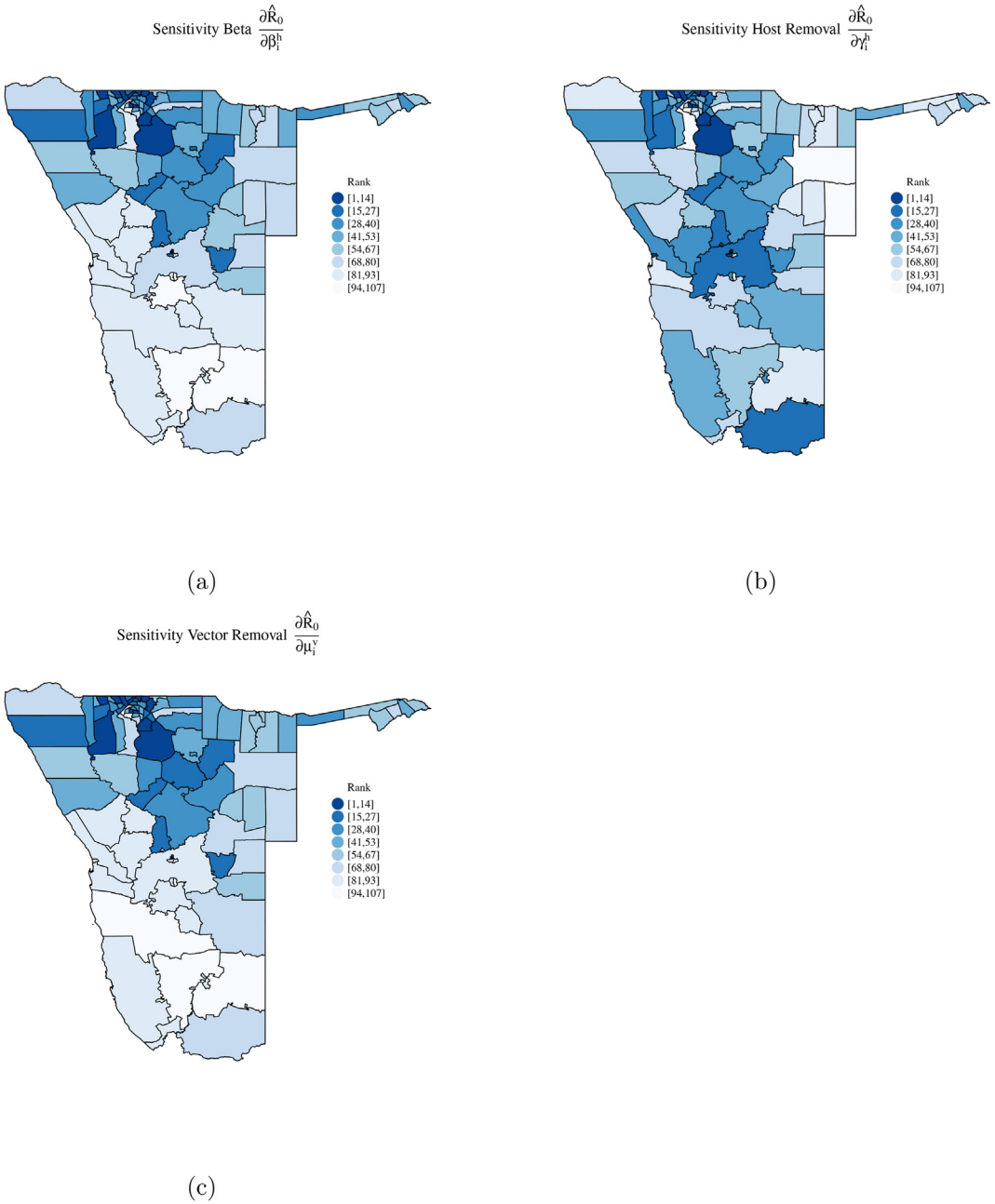

Fig. 6. Comparison of $\hat{\mathcal{R}}_0$ sensitivities to health district parameters. Color corresponds to rank (107 = least sensitive health district, 1 = most sensitive health district). (a) Sensitivities of $\hat{\mathcal{R}}_0$ to β_i^h, calculated from (3.26). (b) Sensitivities of $\hat{\mathcal{R}}_0$ to γ_i^h, calculated from (3.28). (c) Sensitivities of $\hat{\mathcal{R}}_0$ to μ_i^v, calculated from (3.29).

transmission characteristics combine to affect vector-host disease dynamics. As our case study of malaria in Namibia illustrates, these analytical results can be applied to empirical disease settings of public health interest. Closed form expressions approximating the domain $\mathcal{R}_0$ and sensitivities of $\mathcal{R}_0$ to model parameters such as those provided here are important beyond simply the numerical values they provide, as they give insight into the factors underlying $\mathcal{R}_0$ and the parameter sensitivities.

Data on both network connectivity as well as local transmission characteristics are needed to apply the methods presented in this work. The malaria case study in Namibia utilized cell phone data to estimate network connectivity, and disease prevalence data to estimate local transmission parameters. Human mobility data are being collected from diverse sources, including traffic patterns, cell phone data, airflow, navigation app use, social media posts, and more. Detailed data are being collected as well on host demography (Corder, Ferreira, & Gomes, 2020) and vector habitat suitability (Ayala et al., 2009;

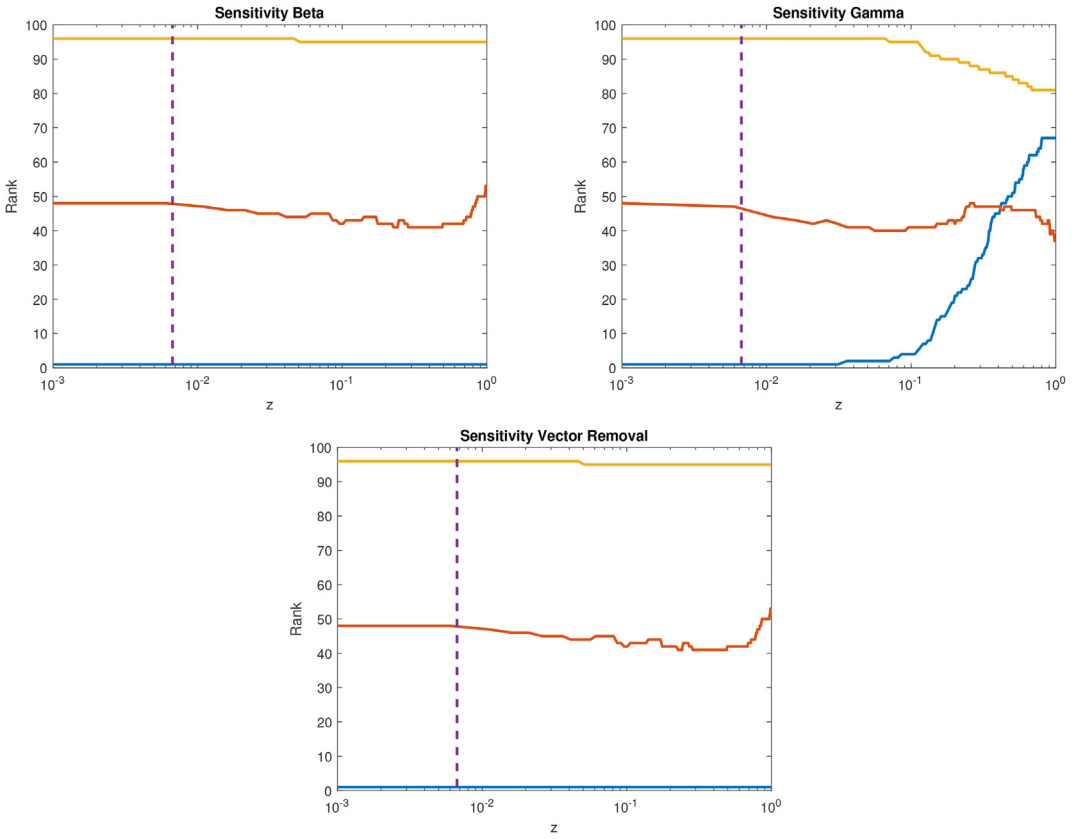

Fig. 7. Rankings of the numerically computed sensitivities of $\hat{\mathcal{R}}_0$ for system (2.1) to patch parameters. The yellow line represents the least sensitive node, the red represents the medium sensitive node, and the blue represents the most sensitive node. The purple dotted line represents the time scale from the data. As the time scale approaches zero, the simulated ranks converge to the analytic rankings.

Chahad-Ehlers, Fushita, Lacorte, de Assis, & Del Lama, 2018). Public repositories will facilitate research on integrating network and local transmission data for understanding disease dynamics.

The techniques presented here build off of methods developed in (Tien et al., 2015) for a patch 'SIWR' model (Tien & Earn, 2010) coupled by environmental pathogen movement. The methodology is flexible and can be applied to a variety of epidemiological models. This includes expansion of system (2.1) to incorporate the movement of vectors, which is an important factor in considering vector-borne diseases (Smith et al., 2004). The scales of movement for host and vector may differ significantly. For example, the typical movement scale for mosquitoes is on the order of a few kilometers (Kaufmann & Briegel, 2004). Although there has been work that has incorporated host and vector movement (Cosner, 2015; Phaijoo & Gurung, 2017), additional studies are needed that merge theoretical concepts with data to understand the interplay of the disease between the host and vector as seen here and in (Vargas Bernal, Saucedo, & Tien, 2022).

The Laurent series (6.4) underlying our analytical results converges for sufficiently small pathogen removal ('absorption') rates. For the malaria in Namibia case study, this criterion is amply met. Indeed, the estimated infectious period is sufficiently long that taking only the lowest order term in the series suffices to give a good approximation. In other situations, additional terms may be needed. For example, a refinement of this work would be to directly estimate the local reproduction numbers for system (2.1) from the Malaria Atlas Project incidence data. We note that for other disease settings, pathogen removal may be fast relative to movement. In this 'weak coupling' regime, a different series expansion for the fundamental matrix may be used. Further study of how disease dynamics vary with coupling strength is an area for future work.

Declaration of competing interest

The authors declare that they have no known competing financial interests or personal relationships that could have appeared to influence the work reported in this paper.

Acknowledgements

The authors acknowledge the support of the Mathematical Biosciences Institute-DMS 1440386 and NSF grant-DMS 1814737. We would like to thank Dr. Nick Ruktanonchai for providing the mobility data that allowed us to conduct the case study in this article.

Appendix. Overview of the Laurent series expansion and $\mathcal{R}_0$

Absorption, movement, and random walks

In this section we provide an overview of the Laurent series approach for approximating the domain reproduction number introduced in (Tien et al., 2015). Further information on this approach can be found in (Jacobsen & Tien, 2018; Tien et al., 2015).

Consider system (2.1) and the domain $\mathcal{R}_0$ according to the next generation matrix approach (van den Driessche & Watmough, 2002). The next generation matrix FV^{-1} involves a matrix V describing the transfer of existing infections. In (2.1), the transfer of existing infection in hosts occurs through either movement or removal (i.e. death or recovery). The mobility network for infected host movement appears in the transfer matrix via the (unnormalized) graph Laplacian L.

As in (Tien et al., 2015), the transfer matrix V has the following block:

$$V_{sub} = L + D, \tag{6.1}$$

where L is the (unnormalized) graph Laplacian for infected host movement, and $D = \text{diag}\{\mu_i^h + \gamma_i^h\}$ corresponds to host removal.

Note that (A1) and (A2) imply that D is full rank, and (A3) together with the preceding discussion give that L has one-dimensional nullspace spanned by u. We will refer to D as the host *absorption* matrix. This appearance of the graph Laplacian plus absorption in the transfer matrix is pervasive in Eulerian modeling frameworks for movement between discrete spatial locations. See (Tien et al., 2015) for an example involving environmental pathogen movement.

For the next generation matrix, we need the inverse of the transfer matrix; hence we will need to invert (6.1). As discussed in (Tien et al., 2015), a key point is the relative magnitudes of movement ($\|L\|$) to absorption ($\|D\|$). Let

$$D = z\overline{D}, \tag{6.2}$$

where

$$\overline{D} = D \Big/ \max_i D_{ii}. \tag{6.3}$$

Thus $z > 0$ is a parameter describing the scale of absorption. We can consider the effect of varying z while the relative absorption rates between nodes is fixed.

For sufficiently small z, $(L + z\overline{D})^{-1}$ can be expressed as a Laurent series. Particularly important here is the *absorption inverse* L^d, described in (Jacobsen & Tien, 2018). As given in (Jacobsen & Tien, 2018), for $|z| < 1/\rho(L^d\overline{D})$, we have

$$(L + z\overline{D})^{-1} = \frac{1}{z}U + L^d + \sum_{k=1}^{\infty} (-zL^d\overline{D})^k L^d, \tag{6.4}$$

where $U = \frac{u\mathbf{1}^T}{\overline{d}}$. Note that the higher order terms of (6.4) depend upon the absorption inverse L^d. The absorption inverse L^d is a generalized inverse of the graph Laplacian, that is closely related to the *absorption-scaled graph* AD^{-1}. The absorption inverse thus integrates features of both the network structure (A) as well as the absorption rates at the nodes (D). For characterization and description of properties of L^d, see (Jacobsen & Tien, 2018); numerical methods for computing L^d are presented in (Benzi, Fika, & Mitrouli, 2019).

The Laurent series (6.4) can be used to derive approximations to $\mathcal{R}_0$ by truncating the series after a desired number of terms. For example, for the network model with environmental pathogen movement studied in (Tien et al., 2015), approximating $\mathcal{R}_0$ using the lowest order term in the Laurent series gave

$$\mathcal{R}_0 \approx \mathrm{E}[\mathcal{R}_{0,i}], \tag{6.5}$$

where $\mathcal{R}_{0,i}$ is the reproduction number of location i in isolation and the expectation is taken with respect to the probability measure $d_i u_i/\overline{d}$, with

$$\overline{d} = \sum_{i=1}^{n} u_i d_i. \tag{6.6}$$

We shall see that this same probability measure features prominently for the vector-borne disease model studied here. We thus mention one way to think about this probability measure: $d_i u_i / \overline{d}$ corresponds both to components of a basis for $\ker L^d$, and to the stationary distribution of the continuous-time random walk generated by the Laplacian of the absorption-scaled graph.

References

Acevedo, M. A., Prosper, O., Lopiano, K., Ruktanonchai, N., Caughlin, T. T., Martcheva, M., et al. (2015). Spatial heterogeneity, host movement and mosquito-borne disease transmission. *PLoS One, 10*(6), Article e0127552.

Adams, B., & Kapan, D. D. (2009). Man bites mosquito: Understanding the contribution of human movement to vector-borne disease dynamics. *PLoS One, 4*(8), 1–10. https://doi.org/10.1371/journal.pone.0006763, 10.1371/journal.pone.0006763. URL.

Agusto, F. B., Del Valle, S. Y., Blayneh, K. W., Ngonghala, C. N., Goncalves, M. J., Li, N., et al. (2013). The impact of bed-net use on malaria prevalence. *Journal of Theoretical Biology, 320*, 58–65. https://doi.org/10.1016/j.jtbi.2012.12.007. URL https://www.sciencedirect.com/science/article/pii/S0022519312006315.

Althouse, B. M., Lessler, J., Sall, A. A., Diallo, M., Hanley, K. A., Watts, D. M., et al. (2012). Synchrony of sylvatic dengue isolations: A multi-host, multi-vector SIR model of dengue virus transmission in Senegal. *PLoS Neglected Tropical Diseases, 6*(11). e1928–e1928. doi:10.1371/journal.pntd.0001928. URL https://pubmed.ncbi.nlm.nih.gov/23209867.

Arino, J., & van den Driessche, P. (2006). Disease spread in metapopulations. *Fields Institute Communications, 48*(1), 1–13.

Aron, J. L., & May, R. M. (1982). The population dynamics of malaria. In R. M. Anderson (Ed.), *The population dynamics of infectious disease: Theory and appplications* (pp. 139–179). London: Chapman and Hall.

Auger, P., Kouokam, E., Sallet, G., Tchuente, M., & Tsanou, B. (2008). The Ross–MacDonald model in a patchy environment. *Mathematical Biosciences, 216*(2), 123–131.

Ayala, D., Costantini, C., Ose, K., Kamdem, G. C., Antonio-Nkondjio, C., Agbor, J.-P., et al. (2009). Habitat suitability and ecological niche profile of major malaria vectors in Cameroon. *Malaria Journal, 8*(1), 307.

Ball, F., Britton, T., House, T., Isham, V., Mollison, D., Pellis, L., et al. (2015). Seven challenges for metapopulation models of epidemics, including household models. *Epidemics, 10*, 63–67.

Barrios, E., Lee, S., & Vasilieva, O. (2018). Assessing the effects of daily commuting in two-patch dengue dynamics: A case study of Cali, Colombia. *Journal of Theoretical Biology, 453*, 14–39. https://doi.org/10.1016/j.jtbi.2018.05.015. URL https://www.sciencedirect.com/science/article/pii/S0022519318302431.

Benzi, M., Fika, P., & Mitrouli, M. (2019). Graphs with absorption: Numerical methods for the absorption inverse and the computation of centrality measures. *Linear Algebra and its Applications, 574*, 123–152.

Berman, A., & Plemmons, R. J. (1994). *Nonnegative matrices in the mathematical sciences*. SIAM.

Bichara, D., & Castillo-Chavez, C. (2016). Vector-borne diseases models with residence times–a Lagrangian perspective. *Mathematical Biosciences, 281*, 128–138.

Bichara, D. M., Iggidr, A., & Yacheur, S. (2021). Effects of heterogeneity and global dynamics of weakly connected subpopulations. *Mathematical Modelling of Natural Phenomena, 16*, 44.

Bisanzio, D., Bertolotti, L., Tomassone, L., Amore, G., Ragagli, C., Mannelli, A., et al. (2010). Modeling the spread of vector-borne diseases on bipartite networks. *PLoS One, 5*(11), Article e13796.

Bomblies, A. (2014). Agent-based modeling of malaria vectors: The importance of spatial simulation. *Parasites & Vectors, 7*(1), 1–10.

Bousema, T., Drakeley, C., Gesase, S., Hashim, R., Magesa, S., Mosha, F., et al. (2010). Identification of hot spots of malaria transmission for targeted malaria control. *The Journal of Infectious Diseases, 201*(11), 1764–1774.

Caraco, T., Duryea, M. C., Glavanakov, S., Maniatty, W., & Szymanski, B. K. (2001). Host spatial heterogeneity and the spread of vector-borne infection. *Theoretical Population Biology, 59*(3), 185–206.

Chahad-Ehlers, S., Fushita, A. T., Lacorte, G. A., de Assis, P. C. P., & Del Lama, S. N. (2018). Effects of habitat suitability for vectors, environmental factors and host characteristics on the spatial distribution of the diversity and prevalence of haemosporidians in waterbirds from three Brazilian wetlands. *Parasites & Vectors, 11*(1), 276.

Chen, S. (2017). Impacts of deforestation on vector-borne disease incidence. *The Journal of Global Health*, Article e1.

Chitnis, N., Hardy, D., & Smith, T. (2012). A periodically-forced mathematical model for the seasonal dynamics of malaria in mosquitoes. *Bulletin of Mathematical Biology, 74*(5), 1098–1124.

Chitnis, N., Hyman, J. M., & Cushing, J. M. (2008). Determining important parameters in the spread of malaria through the sensitivity analysis of a mathematical model. *Bulletin of Mathematical Biology, 70*(5), 1272.

Churakov, M., Villabona-Arenas, C. J., Kraemer, M. U. G., Salje, H., & Cauchemez, S. (2019). Spatio-temporal dynamics of dengue in Brazil: Seasonal travelling waves and determinants of regional synchrony. *PLoS Neglected Tropical Diseases, 13*(4), 1–13. https://doi.org/10.1371/journal.pntd.0007012, 10.1371/journal.pntd.0007012. URL.

D. T. Citron, C. A. Guerra, A. J. Dolgert, S. L. Wu, J. M. Henry, H. M. Sanchez C, D. L. Smith, Comparing metapopulation dynamics of infectious diseases under different models of human movement, Proceedings of the National Academy of Sciences 118 (18). arXiv:https://www.pnas.org/content/118/18/e2007488118.full.pdf, doi:10.1073/pnas.2007488118. URL https://www.pnas.org/content/118/18/e2007488118.

Corder, R. M., Ferreira, M. U., & Gomes, M. G. M. (2020). Modelling the epidemiology of residual *Plasmodium vivax* malaria in a heterogeneous host population: A case study in the Amazon basin. *PLoS Computational Biology, 16*(3), Article e1007377.

Cosner, C. (2015). Models for the effects of host movement in vector-borne disease systems. *Mathematical Biosciences, 270*, 192–197.

Cosner, C., Beier, J. C., Cantrell, R. S., Impoinvil, D., Kapitanski, L., Potts, M. D., et al. (2009). The effects of human movement on the persistence of vector-borne diseases. *Journal of Theoretical Biology, 258*(4), 550–560.

Demers, J., Bewick, S., Agusto, F., Caillouët, K. A., Fagan, W. F., & Robertson, S. L. (2020). Managing disease outbreaks: The importance of vector mobility and spatially heterogeneous control. *PLoS Computational Biology, 16*(8), Article e1008136.

Dobrow, R. P. (2016). *Introduction to stochastic processes with R*. John Wiley & Sons.

Doolan, D. L., Dobaño, C., & Baird, J. K. (2009). Acquired immunity to malaria. *Clinical Microbiology Reviews, 22*(1), 13–36.

van den Driessche, P., & Watmough, J. (2002). Reproduction numbers and sub-threshold endemic equilibria for compartmental models of disease transmission. *Mathematical Biosciences, 180*, 29–48.

Gaff, H. D., & Gross, L. J. (2007). Modeling tick-borne disease: A metapopulation model. *Bulletin of Mathematical Biology, 69*(1), 265–288. https://doi.org/10.1007/s11538-006-9125-5, 10.1007/s11538-006-9125-5. URL.

Gao, D. (2019). Travel frequency and infectious diseases. *SIAM Journal on Applied Mathematics, 79*(4), 1581–1606.

Gao, D., & Ruan, S. (2012). A multipatch malaria model with logistic growth populations. *SIAM Journal on Applied Mathematics, 72*(3), 819–841.

Gao, D., & Ruan, S. (2014). Malaria models with spatial effects. In D. Chen, B. Moulin, & J. Wu (Eds.), *Analyzing and modeling spatial and temporal dynamics of infectious diseases* (pp. 111–138). John Wiley & Sons, Inc.

Gething, P. W., Patil, A. P., Smith, D. L., Guerra, C. A., Elyazar, I. R., Johnston, G. L., et al. (2011). A new world malaria map: *Plasmodium falciparum* endemicity in 2010. *Malaria Journal, 10*(1), 378.
Gueron, S., Levin, S. A., & Rubenstein, D. I. (1996). The dynamics of herds: From individuals to aggregations. *Journal of Theoretical Biology, 182*(1), 85–98.
Guerra, C. A., Reiner, R. C., Perkins, T. A., Lindsay, S. W., Midega, J. T., Brady, O. J., et al. (2014). A global assembly of adult female mosquito mark-release-recapture data to inform the control of mosquito-borne pathogens. *Parasites & Vectors, 7*(1), 276. https://doi.org/10.1186/1756-3305-7-276, 10.1186/1756-3305-7-276. URL.
Hanski, I. (1999). *Metapopulation ecology*. Oxford University Press.
Hasibeder, G., & Dye, C. (1988). Population dynamics of mosquito-borne disease: Persistence in a completely heterogeneous environment. *Theoretical Population Biology, 33*(1), 31–53.
Hay, S. I., Guerra, C. A., Tatem, A. J., Atkinson, P. M., & Snow, R. W. (2005). Urbanization, malaria transmission and disease burden in Africa. *Nature Reviews Microbiology, 3*(1), 81–90.
Horn, R. A., & Johnson, C. R. (1986). *Matrix analysis* (Vol. 1). Cambridge.
Hoshen, M. B., & Morse, A. P. (2004). A weather-driven model of malaria transmission. *Malaria Journal, 3*(1), 32. https://doi.org/10.1186/1475-2875-3-32, 10.1186/1475-2875-3-32. URL.
Hughes, H., & Britton, N. F. (2013). Modelling the use of Wolbachia to control dengue Fever transmission. *Bulletin of Mathematical Biology, 75*(5), 796–818. https://doi.org/10.1007/s11538-013-9835-4, 10.1007/s11538-013-9835-4. URL.
Iggidr, A., Sallet, G., & Souza, M. O. (2016). On the dynamics of a class of multi-group models for vector-borne diseases. *Journal of Mathematical Analysis and Applications, 441*(2), 723–743.
Jacobsen, K. A., & Tien, J. H. (2018). A generalized inverse for graphs with absorption. *Linear Algebra and its Applications, 537*, 118–147.
Jindal, A., & Rao, S. (2017). Agent-based modeling and simulation of mosquito-borne disease transmission. In *Proceedings of the 16th conference on autonomous agents and multiagent systems* (pp. 426–435).
Kaufmann, C., & Briegel, H. (2004). Flight performance of the malaria vectors *Anopheles gambiae* and *Anopheles atroparvus*. *Journal of Vector Ecology, 29*, 140–153.
Kirkland, S., Shuai, Z., van den Driessche, P., & Wang, X. (2021). Impact of varying community networks on disease invasion. *SIAM Journal on Applied Mathematics, 81*(3), 1166–1189. https://doi.org/10.1137/20M1328762. arXiv:.
Lee, S. A., Jarvis, C. I., Edmunds, W. J., Economou, T., & Lowe, R. (2021). Spatial connectivity in mosquito-borne disease models: A systematic review of methods and assumptions. *Journal of The Royal Society Interface, 18*(178), Article 20210096.
Le, P. V., Kumar, P., & Ruiz, M. O. (2018). Stochastic lattice-based modelling of malaria dynamics. *Malaria Journal, 17*(1), 1–17.
Lin, C.-J., Deger, K. A., & Tien, J. H. (2016). Modeling the trade-off between transmissibility and contact in infectious disease dynamics. *Mathematical Biosciences, 277*, 15–24.
Lippi, C. A., Mao, L., Stewart-Ibarra, A. M., Heydari, N., Ayala, E. B., Burkett-Cadena, N. D., et al. (2020). A network analysis framework to improve the delivery of mosquito abatement services in machala, Ecuador. *International Journal of Health Geographics, 19*(1), 1–14.
Maliyoni, M., Chirove, F., Gaff, H. D., & Govinder, K. S. (2017). A stochastic tick-borne disease model: Exploring the probability of pathogen persistence. *Bulletin of Mathematical Biology, 79*(9), 1999–2021.
Manore, C. A., Hickmann, K. S., Hyman, J. M., Foppa, I. M., Davis, J. K., Wesson, D. M., et al. (2015). A network-patch methodology for adapting agent-based models for directly transmitted disease to mosquito-borne disease. *Journal of Biological Dynamics, 9*(1), 52–72. https://doi.org/10.1080/17513758.2015.1005698. pMID: 25648061. arXiv:.
Marino, S., Hogue, I. B., Ray, C. J., & Kirschner, D. E. (2008). A methodology for performing global uncertainty and sensitivity analysis in systems biology. *Journal of Theoretical Biology, 254*(1), 178–196.
Matthys, B., Vounatsou, P., Raso, G., Tschannen, A. B., Becket, E. G., Gosoniu, L., et al. (2006). Urban farming and malaria risk factors in a medium-sized town in Cote d'Ivoire. *The American Journal of Tropical Medicine and Hygiene, 75*(6), 1223–1231.
Mbogo, C. M., Mwangangi, J. M., Nzovu, J., Gu, W., Yan, G., Gunter, J. T., et al. (2003). Spatial and temporal heterogeneity of *Anopheles* mosquitoes and *Plasmodium falciparum* transmission along the Kenyan coast. *The American Journal of Tropical Medicine and Hygiene, 68*(6), 734–742.
Mniszewski, S. M., Manore, C., Bryan, C., Del Valle, S. Y., & Roberts, D. (2014). Towards a hybrid agent-based model for mosquito borne disease. In *Summer computer simulation conference:(SCSC 2014): 2014 summer simulation multi-conference: Monterey, California, USA, 6-10 july 2014. Summer computer simulation conference (2014: Monterey, calif.)* (Vol. 2014)NIH Public Access.
Mpolya, E. A., Yashima, K., Ohtsuki, H., & Sasaki, A. (2014). Epidemic dynamics of a vector-borne disease on a villages-and-city star network with commuters. *Journal of Theoretical Biology, 343*, 120–126. https://doi.org/10.1016/j.jtbi.2013.11.024. URL https://www.sciencedirect.com/science/article/pii/S0022519313005511.
Mukhtar, A. Y., Munyakazi, J. B., & Ouifki, R. (2020). Assessing the role of human mobility on malaria transmission. *Mathematical Biosciences, 320*, Article 108304. https://doi.org/10.1016/j.mbs.2019.108304. URL https://www.sciencedirect.com/science/article/pii/S0025556419305450.
Paton, D. G., Childs, L. M., Itoe, M. A., Holmdahl, I. E., Buckee, C. O., & Catteruccia, F. (2019). Exposing *Anopheles* mosquitoes to antimalarials blocks *Plasmodium* parasite transmission. *Nature, 567*(7747), 239–243. https://doi.org/10.1038/s41586-019-0973-1, 10.1038/s41586-019-0973-1. URL.
Pei, S., Kandula, S., & Shaman, J. (2020). Differential effects of intervention timing on COVID-19 spread in the United States. *Science Advances, 6*(49). https://doi.org/10.1126/sciadv.abd6370. eabd6370. arXiv:https://www.science.org/doi/pdf/10.1126/sciadv.abd6370.
Phaijoo, G. R., & Gurung, D. B. (2017). Modeling impact of temperature and human movement on the persistence of dengue disease. *Computational and Mathematical Methods in Medicine, 17*, 1–9.
Statista Plecher, H. (2018). Namibia- statistics and facts. e1 https://www.statista.com/topics/4038/namibia/.
Qiu, Z., Kong, Q., Li, X., & Martcheva, M. (2013). The vector-host epidemic model with multiple strains in a patchy environment. *Journal of Mathematical Analysis and Applications, 405*(1), 12–36.
Reiner, R. C., Jr., Perkins, T. A., Barker, C. M., Niu, T., Fernando Chaves, L., Ellis, A. M., et al. (2013). A systematic review of mathematical models of mosquito-borne pathogen transmission: 1970-2010. *Journal of The Royal Society Interface, 10*, Article 20120921.
Rodriguez, D. J., & Torres-Sorando, L. (2001). Models of infectious diseases in spatially heterogeneous environments. *Bulletin of Mathematical Biology, 63*(3), 547–571.
Rohani, P., Earn, D. J., & Grenfell, B. T. (1999). Opposite patterns of synchrony in sympatric disease metapopulations. *Science, 286*(5441), 968–971.
Ross, R. (1916). An application of the theory of probabilities to the study of *a priori* pathometry. Part I. *Proceedings of the Royal Society of London, Series A, 92*, 204–230.
Ruktanonchai, N. W., DeLeenheer, P., Tatem, A. J., Alegana, V. A., Caughlin, T. T., zu Erbach-Schoenberg, E., et al. (2016b). Identifying malaria transmission foci for elimination using human mobility data. *PLoS Computational Biology, 12*(4), 1–19.
Ruktanonchai, N., Smith, D. L., & De Leenheer, P. (2016a). Parasite sources and sinks in a patched Ross-MacDonald malaria model with human and mosquito movement: Implications for control. *Mathematical Biosciences, 279*, 90–101.
Schwab, S. R., Stone, C. M., Fonseca, D. M., & Fefferman, N. H. (2018). The importance of being urgent: The impact of surveillance target and scale on mosquito-borne disease control. *Epidemics, 23*, 55–63. https://doi.org/10.1016/j.epidem.2017.12.004. URL https://www.sciencedirect.com/science/article/pii/S1755436517301317.
Smith, D. L., Battle, K. E., Hay, S. I., Barker, C. M., Scott, T. W., & McKenzie, F. E. (2012). Ross, MacDonald, and a theory for the dynamics and control of mosquito-transmitted pathogens. *PLoS Pathogens, 8*(4), Article e1002588.
Smith, D. L., Dushoff, J., & McKenzie, F. E. (2004). The risk of a mosquito-borne infection in a heterogeneous environment. *PLoS Biology, 2*(11), Article e368.

Smith, D. L., Perkins, T. A., Reiner, J., Robert, C., Barker, C. M., Niu, T., et al. (2014). Recasting the theory of mosquito-borne pathogen transmission dynamics and control. *Transactions of The Royal Society of Tropical Medicine and Hygiene, 108*(4), 185–197. https://doi.org/10.1093/trstmh/tru026. arXiv:https://academic.oup.com/trstmh/article-pdf/108/4/185/5425936/tru026.pdf.

Son, H., & Denu, D. (2021). Vector-host epidemic model with direct transmission in random environment, Chaos. *An Interdisciplinary Journal of Nonlinear Science, 31*(11), Article 113117.

Stoddard, S. T., Morrison, A. C., Vazquez-Prokopec, G. M., Soldan, V. P., Kochel, T. J., Kitron, U., et al. (2009). The role of human movement in the transmission of vector-borne pathogens. *PLoS Neglected Tropical Diseases, 3*(7), Article e481.

Sumner, T., Orton, R. J., Green, D. M., Kao, R. R., & Gubbins, S. (2017). Quantifying the roles of host movement and vector dispersal in the transmission of vector-borne diseases of livestock. *PLoS Computational Biology, 13*(4), Article e1005470.

Sutherst, R. W. (2004). Global change and human vulnerability to vector-borne diseases. *Clinical Microbiology Reviews, 17*(1), 136–173.

Tatem, A. J., Huang, Z., Narib, C., Kumar, U., Kandula, D., Pindolia, D. K., et al. (2014). Integrating rapid risk mapping and mobile phone call record data for strategic malaria elimination planning. *Malaria Journal, 13*, 52.

Tibayrenc, M. (2017). *Genetics and evolution of infectious diseases*. Elsevier.

Tien, J. H., & Earn, D. J. (2010). Multiple transmission pathways and disease dynamics in a waterborne pathogen model. *Bulletin of Mathematical Biology, 72*(6), 1506–1533.

Tien, J. H., Shuai, Z., Eisenberg, M. C., & van den Driessche, P. (2015). Disease invasion on community networks with environmental pathogen movement. *Journal of Mathematical Biology, 70*(5), 1065–1092.

Torres-Sorando, L., & Rodriguez, D. J. (1997). Models of spatio-temporal dynamics in malaria. *Ecological Modelling, 104*(2–3), 231–240.

Vargas Bernal, E., Saucedo, O., & Tien, J. H. (2022). Relating Eulerian and Lagrangian spatial models for vector-host disease dynamics through a fundamental matrix. *Journal of Mathematical Biology, 84*(57).

Wang, W. (2007). Epidemic models with population dispersal. In *Mathematics for life science and medicine* (pp. 67–95). Springer.

Xia, Y., Bjørnstad, O. N., & Grenfell, B. T. (2004). Measles metapopulation dynamics: A gravity model for epidemiological coupling and dynamics. *The American Naturalist, 164*(2), 267–281.

Zhang, R. (2020). Global dynamic analysis of a model for vector-borne diseases on bipartite networks. *Physica A: Statistical Mechanics and its Applications, 545*, Article 123813.

Zhao, R., Liu, Q., & Zhang, H. (2021). Dynamical behaviors of a vector-borne diseases model with two time delays on bipartite networks. *Mathematical Biosciences and Engineering, 18*(4), 3073–3091.